ARMY RESEARCH LABORATORY

Metallographic Observations of Rolled-Homogeneous-Armor Specimens From Plates Perforated by Shaped Charge Jets

Claire D. Krause
Martin N. Raftenberg

ARL-MR-68 June 1993

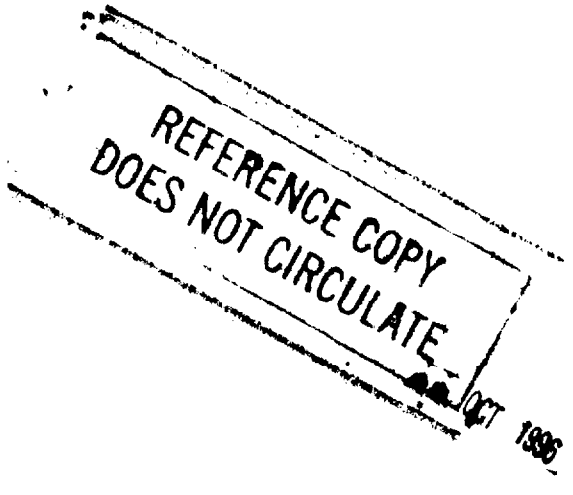

NOTICES

Destroy this report when it is no longer needed. DO NOT return it to the originator.

Secondary distribution of this report is prohibited.

Additional copies of this report may be obtained from the Defense Technical Information Center, Cameron Station, Alexandria, VA 22304-6145.

The findings of this report are not to be construed as an official Department of the Army position, unless so designated by other authorized documents.

The use of trade names or manufacturers' names in this report does not constitute indorsement of any commercial products.

REPORT DOCUMENTATION PAGE

Form Approved
OMB No. 0704-0188

1. AGENCY USE ONLY (Leave blank)	2. REPORT DATE	3. REPORT TYPE AND DATES COVERED
	June 1993	Final, November 1988–November 1992

4. TITLE AND SUBTITLE

Metallographic Observations of Rolled-Homogeneous-Armor Specimens From Plates Perforated by Shaped Charge Jets

5. FUNDING NUMBERS

PR: 1L162618AH80

6. AUTHOR(S)

Claire D. Krause and Martin N. Raftenberg

7. PERFORMING ORGANIZATION NAME(S) AND ADDRESS(ES)

U.S. Army Research Laboratory
ATTN: AMSRL-WT-TD
Aberdeen Proving Ground, MD 21005-5066

8. PERFORMING ORGANIZATION REPORT NUMBER

9. SPONSORING/MONITORING AGENCY NAME(S) AND ADDRESS(ES)

U.S. Army Research Laboratory
ATTN: AMSRL-OP-CI-B (Tech Lib)
Aberdeen Proving Ground, MD 21005-5066

10. SPONSORING/MONITORING AGENCY REPORT NUMBER

ARL-MR-68

11. SUPPLEMENTARY NOTES

Comments should be referred to Dr. Raftenberg at U.S. Army Research Laboratory, ATTN: AMSRL-WT-TD, Aberdeen Proving Ground, MD 21005-5066.

12a. DISTRIBUTION/AVAILABILITY STATEMENT

Approved for public release; distribution is unlimited.

12b. DISTRIBUTION CODE

13. ABSTRACT *(Maximum 200 words)*

In each of a series of experiments, a plate of rolled homogeneous armor (RHA) is perforated by a copper jet from a shaped charge warhead. Microscopy specimens of RHA are prepared from a remaining, perforated target plate and from various recovered fragments. Optical and scanning electron microscopy reveal shear bands, voids, cracks, and evidence of precipitate formation and microstructure transformation in the original martensite. Some shear bands contain a finer-scaled microstructure than that of the ambient martensite, while others contain martensitic laths of dimensions similar to those of the ambient martensite. Cracks in RHA specimens are generally associated either with shear bands or with coalescing voids. In a specimen from a copper fragment, a variety of grain sizes and extensive twinning are observed.

14. SUBJECT TERMS	15. NUMBER OF PAGES
shaped charge warhead; rolled homogeneous armor; fragmentation; shear bands; damage	42
	16. PRICE CODE

17. SECURITY CLASSIFICATION OF REPORT	18. SECURITY CLASSIFICATION OF THIS PAGE	19. SECURITY CLASSIFICATION OF ABSTRACT	20. LIMITATION OF ABSTRACT
UNCLASSIFIED	UNCLASSIFIED	UNCLASSIFIED	UL

INTENTIONALLY LEFT BLANK.

ACKNOWLEDGMENTS

The authors would like to recognize the efforts of several staff members of the U.S. Army Research Laboratory. Dr. Pat Kingman assisted with the use of the scanning electron microscope. Mr. David E. Mackenzie helped with the preparation of specimens for microscopy. The range firing at Range 7A was performed by Messrs. Grat E. Blackburn, David R. Schall, and Sterling C. Shelley, Jr. The three firings at Range 16 were performed by Messrs. Carl V. Paxton and Joseph W. Gardiner. Dr. Lee S. Magness provided a very helpful review of the manuscript.

INTENTIONALLY LEFT BLANK.

TABLE OF CONTENTS

INTENTIONALLY LEFT BLANK.

LIST OF FIGURES

LIST OF TABLES

INTENTIONALLY LEFT BLANK.

1. INTRODUCTION

Four experiments are performed, in each of which a shaped charge warhead is fired at normal incidence into a plate of rolled homogeneous armor (RHA). The same type of warhead is used in all experiments. The two parameters varied in the series are the standoff, or distance between charge base and the target plate, and the target plate thickness. Metallographic observations of RHA specimens from a perforated target plate from one experiment and from recovered fragments from the other three experiments will be presented. Both optical and scanning electron micrographs will reveal the presence of five features that presumably resulted from the penetration event: (i) shear bands, (ii) voids, (iii) cracks, (iv) precipitates, and (v) evidence of changes in the martensitic microstructure.

Two companion reports (Raftenberg 1992, to be published) present other data from these same four experiments. These data include: (i) flash radiographs, both of the jet prior to impact and of the behind-armor-debris pattern at specific times following perforation; (ii) measurements pertaining to the final geometry of the target plate hole; (iii) measurements of the total mass lost by the target plate; (iv) observations of the fracture surface pattern near the target plate hole; and (v) geometrical observations on the largest recovered fragments. Together, the three reports are intended to provide an overview of the physics of RHA plate perforation by a shaped charge jet.

Section 2 of this report will describe the four experiments from which RHA specimens were obtained. Also described here are the specimen preparation procedure and the optical microscope and scanning electron microscope (SEM) employed. Section 3 presents metallographic observations of the RHA specimens. Specifically, Subsection 3.1 is devoted to specimens prepared from a perforated target plate, and Subsection 3.2 to specimens prepared from recovered fragments. Section 4 follows with a discussion of the results.

2. METHODS

The shaped charge warhead used throughout the four experiments is described in Raftenberg (to be published). This warhead contains a conical liner composed of OFHC copper and has a vertex angle of 42°. The jet tip speed produced by this warhead has been determined to be 7.73 mm/μs (Raftenberg 1992; Raftenberg and Krause 1992).

The target plates are composed of RHA, a quenched and tempered, medium-carbon, martensitic steel (U. S. Department of Defense 1984). Each has a square cross section, with an edge length of either 197 mm or about 254 mm. Two values for target plate thickness d are considered: 13 and 25 mm. The Brinell hardness is measured at a single location on each of the entrance and exit surfaces. These measurements are denoted $BHN_{ent.}$ and BHN_{exit}, respectively.

Figure 1 displays the setup employed in the series of experiments. The warhead is supported on a horizontal platform containing a hole through which the jet can pass. Four vertical bolts are attached to the underside of this platform. The target plate is suspended from these bolts by means of a hook welded to each of its four edges. The plate's square cross section is oriented horizontally, so that the jet strikes at normal incidence. Standoff S is controlled by adjusting the elevation of the target plate's attachment to these bolts and by elevating the warhead by means of a wooden stand. Three values of standoff are considered: 3.00 charge diameters (C.D.), or 244 mm; 12.00 C.D., or 975 mm; and 15.23 C.D., or 1238 mm.

The setup includes x-ray tubes and associated film cassettes. These are described in Raftenberg (1992, to be published). A witness pack is located 609.6 mm beneath the exit surface of the target plate. The pack consists of five mild steel plates and four styrofoam spacers. Each steel plate and spacer has a square cross section with an edge length of about 1219 mm. The thickness of each styrofoam spacer is 25.4 mm. Thicknesses of the steel witness plates, in the order of increasing distance from the target plate, are 0.8, 0.8, 1.6, 1.6, and 3.2 mm. The witness pack is used to collect fragments of RHA and copper and is disassembled for their retrieval following the experiment.

Table 1 presents the values for d, S, cross-sectional dimensions, $BHN_{ent.}$, and BHN_{exit} applicable to each experiment. Each experiment is identified by a round (Rd.) number and has been performed on the indicated date and at the indicated range, either 7A or 16. Each d value has been obtained at a single point near the center of the plate by means of a micrometer.

Figure 2 contains a series of radiographs from Rd. 4099 and another experiment involving the same conditions of 13 mm for d and a 3.00 C.D. standoff. (No fragments were collected from this other experiment, so it has not been included in Table 1.) Figure 2 shows that at this relatively short standoff, the copper jet is still intact and

stretching at the time of initial impact and throughout the course of perforation. In contrast, Figure 3 shows from Rd. 4100 that at the longer standoff of 12.00 C.D., the jet has broken up into particles prior to initial impact. Figure 2 also shows post-perforation debris patterns at five times. At the early times of 17.7 and 33.1 μs after impact, fragments are small and clustered into a dense *debris cloud*. At the three later times, much larger fragments are apparent. This same general pattern of debris was observed throughout the series of experiments.

In the case of Rd. 10771, the perforated RHA plate is sectioned into wedges following the experiment (Figure 4). Microscopy specimens are prepared from thin slices removed from the exposed faces of the tips of the wedges. Specimens from Rd. 10771 are mounted in a bakelite resin. In the case of Rds. 4098, 4099 and 4100, witness packs are disassembled following the experiment, and assorted fragments of RHA are recovered. Recovered fragments are sectioned to expose an internal surface and mounted in a clear epoxy. Specimens from the four experiments are then ground, polished, and etched in a 2% nital solution for approximately ten seconds.

Optical microscopy is performed with a Zeiss Axiomat IAC, an inverted reflected light microscope. The SEM used is a JEOL JXA-840A. Vickers and Rockwell C hardness measurements are obtained on one fragment specimen by means of a LECO M-400 microhardness tester.

3. OBSERVATIONS

3.1 Perforated RHA Plate from Rd. 10771. Figure 5 shows the slice from the wedge of Rd. 10771 from which all micrographs in this subsection are obtained. Figure 6 shows the microstructure of the tempered martensite observed in much of the RHA near the perforation hole boundary.

Crack # 1 shown in Figure 5, emanating from the hole boundary and inclined at about 30° to the shot line, is focused upon first.* This crack extends for about 0.75 mm (Figure 7). It is surrounded by fine-grained material identified as a shear band

* The term *crack* is used in this report to connote *fracture surface*. No implication is made about the degree of brittleness or the applicability of a Griffith theory.

(Figure 8). This shear band continues beyond the tip of the crack. An enlargement of the crack tip region is contained in Figure 9. The four dark spheroidal regions in this figure are presumably either precipitates or cavities left by the removal of precipitates during polishing. A scanning electron micrograph of the same shear band at 3,700x magnification reveals its details (Figure 10). The band's width is 6 μm. The martensitic laths adjacent to the band show some alignment with the band. Structure in the central portion of the band is very fine and difficult to resolve in Figure 10.

Crack #2 in Figure 5 is also inclined at about 30° to the shot line. This crack's width varies greatly with distance along its length (Figure 11). It is not bounded by a fine-grained shear band, as was the first crack. However, a shear band is observed in the vicinity of this second crack's tip.

Two additional shear bands within the RHA plate are now examined. Figure 12 contains a scanning electron micrograph of a shear band at a magnification similar to that of Figure 10. In contrast to that previous figure, in Figure 12 the structure within the shear band does not differ so sharply from that of the ambient martensite. Individual laths are seen to enter the shear band. Figure 13 shows a shear band for which one end terminates on a crack, while the other end fans out and blends into the surrounding structure.

Figure 14 shows a crack that has formed by the coalescence of three voids on the slice shown in Figure 5. These voids range in diameter from 1 to 3 μm. Note the local alignment of martensitic laths along the crack.

3.2 RHA Fragments from Rds. 4098, 4099, and 4100. The witness packs from Rds. 4098, 4099, and 4100 are disassembled following the experiment, and individual fragments are recovered. Figure 15 shows an RHA fragment from Rd. 4099 to be composed largely of lower bainite. This gives evidence that some RHA material near the path of the jet has undergone a change in microstructure from that of its original tempered martensite.

Figure 16 from Rd. 4098 shows a pattern that is familiar from Rd. 10771. A crack beginning at the fragment's outer surface ends at a straight shear band. As in Figures 7 through 9, much of the crack's boundary in Figure 16 is lined by "white"-etching material. This is probably evidence that the crack propagated into previously shear-banded material.

On the other hand, Figure 17 shows shear bands that are not straight, but instead meander around the cross section of this fragment from Rd. 4100. Two of these bands are continuous with a wider shear band that surrounds the fragment. Figure 18 from Rd. 4099 displays a shear band that both bifurcates and abruptly changes direction. The band thickens near its bifurcation point. This region is enlarged in Figure 19.

In Figure 20 from Rd. 4099, the fine-grained band near the fragment's periphery includes a dendritic structure. Figure 21 contains an enlargement. Individual dendrites are oriented approximately orthogonally to the fragment's local boundary. Vickers and Rockwell C hardness measurements are made across the fragment. Indentations from the measurements are visible in Figure 20. Table 2 contains the results. Here VHN and R_C denote Vickers and Rockwell C hardness measurements, respectively. In this table, points are numbered in the order of increasing distance from the fragment's boundary. Vickers hardness is seen to increase from a level of about 350 in the ambient RHA to 483 within the whitened shear band. An intermediate value of 450 is found for the band of dendrites. The dimension of the indentation exceeds a dendrite's width, so a spatial averaging of hardness has occurred in this last measurement. Figure 22 is a scanning electron micrograph of dendrites at 10,000x magnification.

Figure 23 shows a band of striations that follows the boundary of a fragment from Rd. 4099. The total width of the band is about 45 μm. This phenomenon appears to be distinct from both the shear banding and the dendritic structure that have been noted above.

Finally, a single copper fragment from the warhead's liner is shown in Figure 24. This fragment from Rd. 4099 was etched for 10 seconds in a potassium dichromate solution. A variety of grain sizes and a large amount of twinning are both evident.

4. DISCUSSION

The observations in Section 3 have included shear bands, voids, cracks, precipitates, and evidence of changes in martensitic microstructure in RHA and twinning in OFHC copper. These features probably resulted directly from the target plate perforation, although it is possible that the witness pack itself inflicted further damage on some fragments. Each recovered fragment perforated one or more thin sheets of mild steel within the witness pack.

Cracks have been seen to occur in association with shear bands, as in Figures 7 through 9, 11 and 13, and with void coaslescence, as in Figure 14. The mechanism for the association in the case of shear bands is not clear and is probably not consistent. One possibility is the increase in hardness within a shear band relative to that of the surrounding martensite, which was documented in AISI 4340 steel by Rogers and Shastry (1981). This hardness increase is presumably accompanied by an increase in brittleness, thereby lowering the local fracture toughness and predisposing the shear-banded material to fracture. The above scenario supposes that the shear band preceded the crack.

Various observations in Section 3 will now be placed in the context of some recent literature. Rogers and Shastry (1981) formed shear bands in 4340 steel and related alloys by means of impact with flat-nosed projectiles at the relatively low speeds of 0.030 to 0.076 mm/μs. Their observations on shear bands were qualitatively similar to those described above, which correspond to the much greater projectile velocity of 7.73 mm/μs. They called fine-structured shear bands that etch "white" in nital, such as the shear band in Figures 7 through 10, *transformed bands*. They hypothetized that the steel within such a band has undergone a sufficient temperature rise to cause re-austenitization, followed by re-quenching. Rogers and Shastry supported this hypothesis with measurements of increased microhardness within the band. In fact, they claimed the microhardness in transformed bands to be greater than that obtainable by a martensitic transformation brought on by conventional quench and tempering techniques. They attributed the additional increase in microhardness to the extreme reduction in grain size and the thorough dissolution of carbon into the hot austenite, followed by carbon precipitation. This same paper by Rogers and Shastry called shear bands such as that in Figure 12 *deformed bands*. These "are more ill defined regions of high local shear strain with no comparable signature of temperature attained." Rogers and Shastry found microhardness to be much lower here than in the transformed bands. Moreover, they stated that frequently "deformed bands act as 'precursor bands' to transformed bands," on the basis of their observations of situations similar to that in Figure 13.

More recent work by Beatty et al. (1990) casts doubt on the assumption by Rogers and Shastry of local phase transformation within "white"-etching bands, however. Beatty and co-workers generated shear bands in a hat-shaped specimen of VAR 4340 steel by means of a split Hopkinson compression bar technique. By use of transmission electron microscopy (TEM), they obtained selected area diffraction patterns within "white"-etching bands and in the surrounding martensite. The diffraction pattern was found to vary

gradually with distance from the center of the shear band, with no clear discontinuity occurring at the band's periphery. Also, they were unable to find remaining austenite within the bands.

Wittman et al. (1990) produced shear bands in a hollow cylinder of AISI 4340 steel by detonating an explosive charge along its axis. They reported observations similar to those in Beatty et al. (1990): a significant degree of similarity between TEM diffraction patterns inside and outside the shear band and an absence of austenite within the shear band. Furthermore, Wittman and co-workers provided a thermal analysis to suggest that re-austenization within a shear band is avoided because of short time duration (less than 1 ms) at the highest temperatures. Figure 6 of their paper indicates a "white"-etching shear band width of 6 μm, in agreement with Figure 10 of the present report. Also, their Figure 5 illustrates the phenomenon of shear band bifurcation and bears resemblance to Figure 18 of the present report.

Thus, results in Beatty et al. (1990) and Wittman et al. (1990) point to a negative answer to the question of whether or not re-austenization occurs within a "white"-etching shear band in RHA. The lower bainite found in the fragment shown in Figure 15 raises the related question of whether re-austenization occurs in fragmented RHA material that does not undergo shear banding.

Figure 23 shows striations along a boundary of an RHA fragment. The separation between adjacent striations is roughly 20 μm. The total width of the band of striations varies along the fragment's boundary, with a typical value of 400 μm. This pattern of striations is reminiscent of the *flow lines* which according to Hertzberg (1976) are produced by the process of *mechanical fibering* during forging procedures. He defines mechanical fibering to be "the alignment of the grain structure in the direction of mechanical working." On the other hand, the pattern of striations in Figure 23 also bears resemblance to the *reference bands* that Moss (1981) observed in an RHA plate prior to impact. Moss stated that these striations "were planar chemical inhomogeneities that had been spread through the plate as it was rolled from an ingot. They were extraordinarily plane and parallel with the flat surfaces of the disc shaped sample." In fact, Moss used the rotation induced in these striations by penetration of his specimen by a punch as a measure of the shear strain field in the specimen. Thus, the question of whether the striations in Figure 23 were created by the deformation associated with perforation or instead were pre-existent in the plate prior to impact and merely distorted by the

deformation cannot be resolved at this time. However, in favor of the former possibility are the facts that the band of striations in Figure 23 only occurs along the boundary of the fragment shown and that no such pattern is observed in any other specimens prepared from the target plate of Rd. 10771 or recovered fragments from Rds. 4098, 4099, and 4100.

The evidence of spheroidal precipitates that has been noted in Figure 9 can perhaps be identified with the carbon-rich precipitates noted in Glass and Bruchey (1987). Honeycombe (1981) discusses "coarse spheroidized particles of Fe_3C" (cementite) that are found in martensite tempered at above 620 K. The rather large 5-μm dimension of these particles suggests that they more likely formed during the original tempering of the target plate rather than subsequently as a result of the plate's penetration.

The twins observed in the copper specimen of Figure 24 appear to illustrate the phenomenon of *annealing twins* that is described in Meyers and Chawla (1984). There annealing twins are said to be common in FCC metals and are defined as twins that are "formed during heat treatment (recovery, recrystallization, and grain growth)," rather than as a direct result of mechanical shearing deformation. In the present context, the copper was subjected to intense temperature rise associated with the processes of liner collapse and target interaction, followed by quenching at ambient temperature.

This report has documented isolated observations of microstructural phenomena in RHA material that has undergone perforation by a shaped charge jet. The relevance to this problem of laboratory experiments performed at relatively low strain rates can be judged by determining whether similar phenomena are present. A complete overview of the likelihood of occurrence of shear banding, cracking, void formation, and phase transformation in a perforated plate as functions of position and time has yet to emerge, however. Such an overview on the micromechanical level would be very useful to those modelers attempting to treat this problem in detail.

Table 1. Round Descriptions

Rd.	Date	Range	d (mm)	$BHN_{ent.}$	BHN_{exit}	X-sect. (mm^2)	S (C.D.)
4098	21/06/89	16	25.5	364	364	254x256	3.00
4099	22/06/89	16	12.5	364	340	251x252	3.00
4100	23/06/89	16	25.6	364	340	251x252	12.00
10771	9/11/88	7A	13.0	364	364	197x197	15.23

Table 2. Vickers and Rockwell C Hardness Measurements Across the RHA Fragment of Figures 20, 21, and 22 (100 g Load Used)

Pt.	VHN	R_C	Comments
1	373	38.0	two-phase region
2	429	43.5	two-phase region
3	464	46.5	on white shear band
4	483	48.0	on white shear band
5	450	45.3	on dendrite arms
6	450	45.3	on dendrite arms
7	363	36.8	martensite matrix
8	363	36.8	martensite matrix
9	363	36.8	martensite matrix
10	345	35.0	martensite matrix
11	333	33.5	martensite matrix
12	351	35.6	martensite matrix

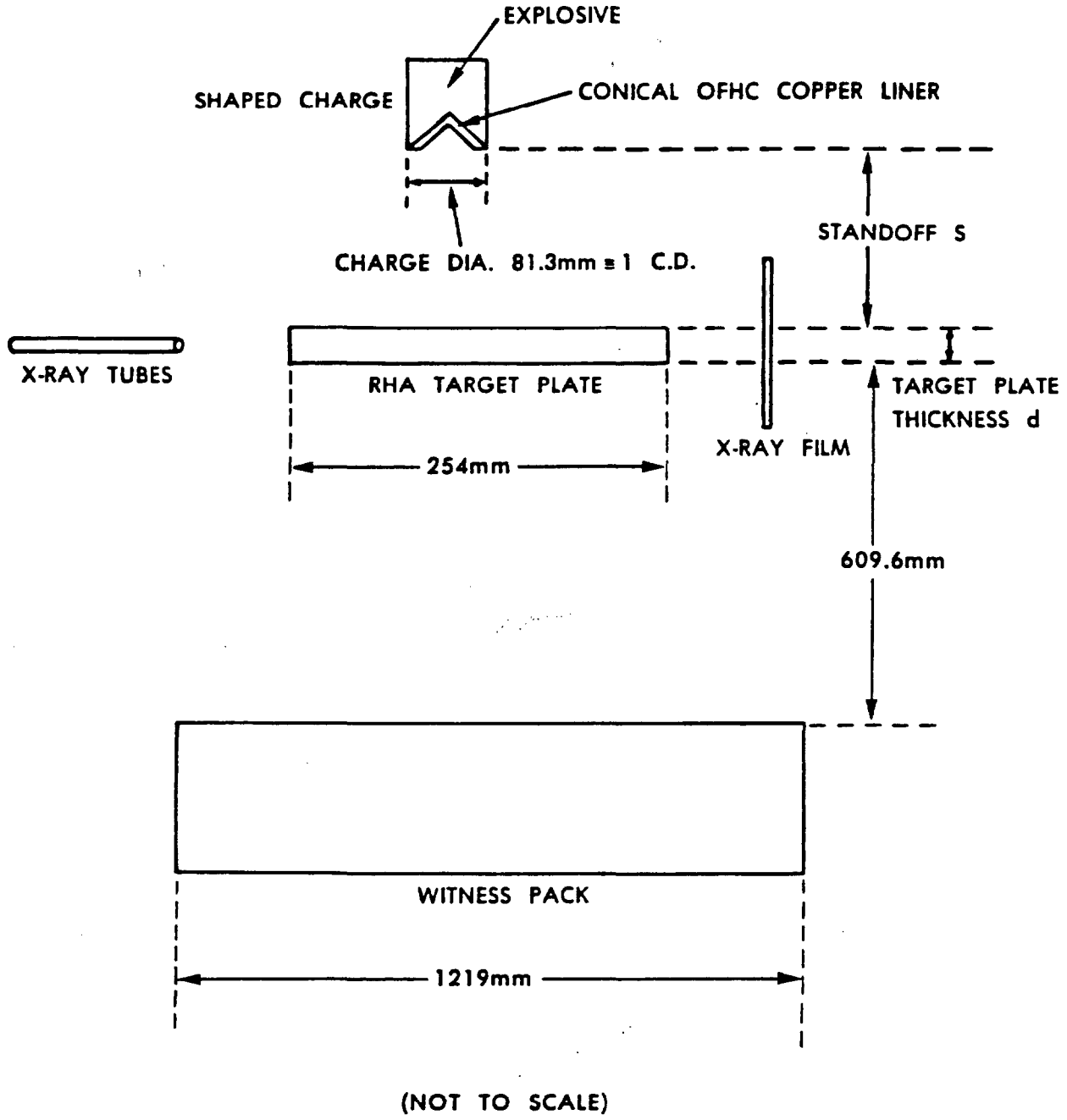

Figure 1. Setup for range firings.

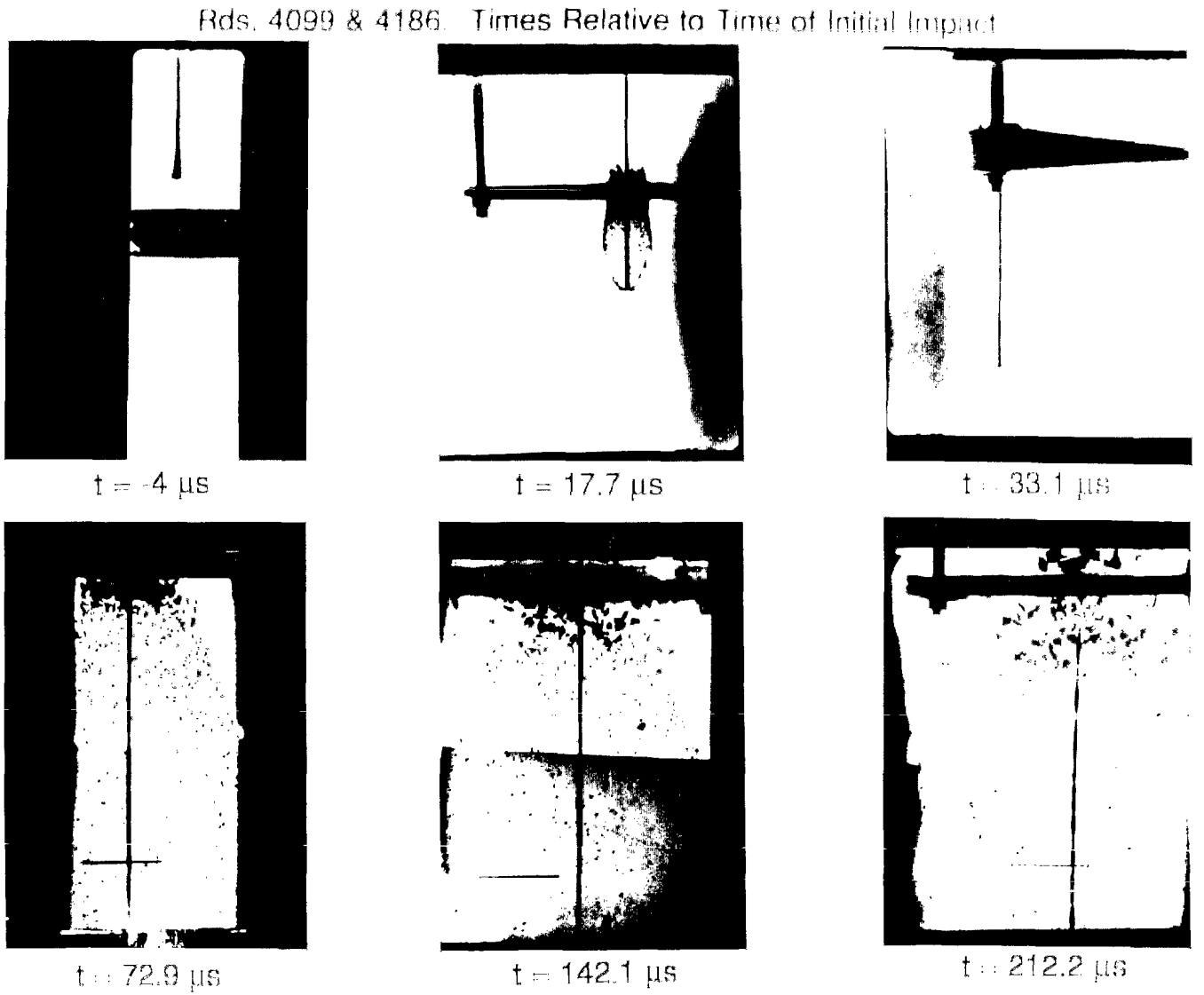

Figure 2. Pre-impact and post-perforation radiographs for a standoff of 3.00 C.D. and a target plate thickness of 13 mm.

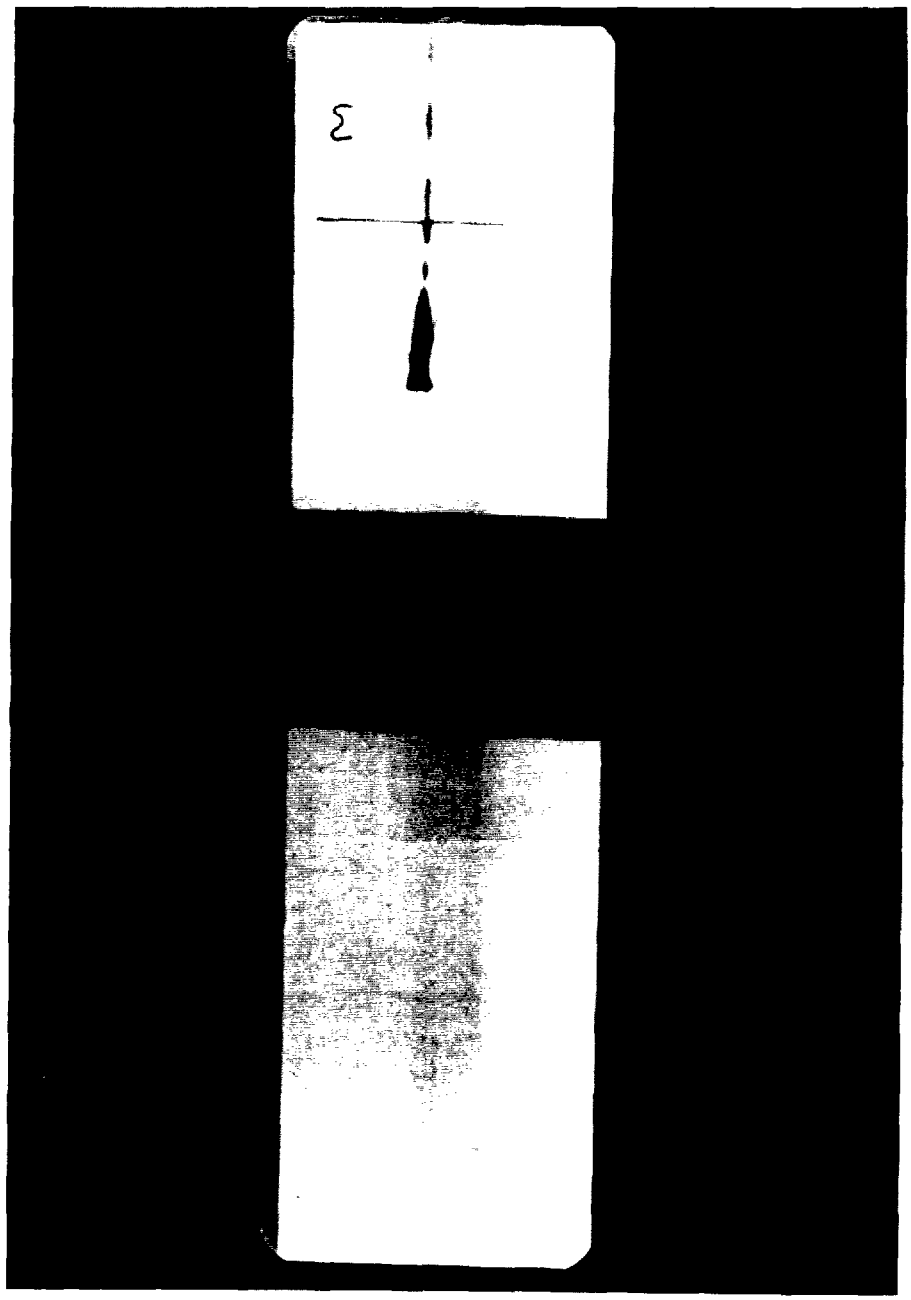

Figure 3. Pre-impact radiograph from Rd. 4100.

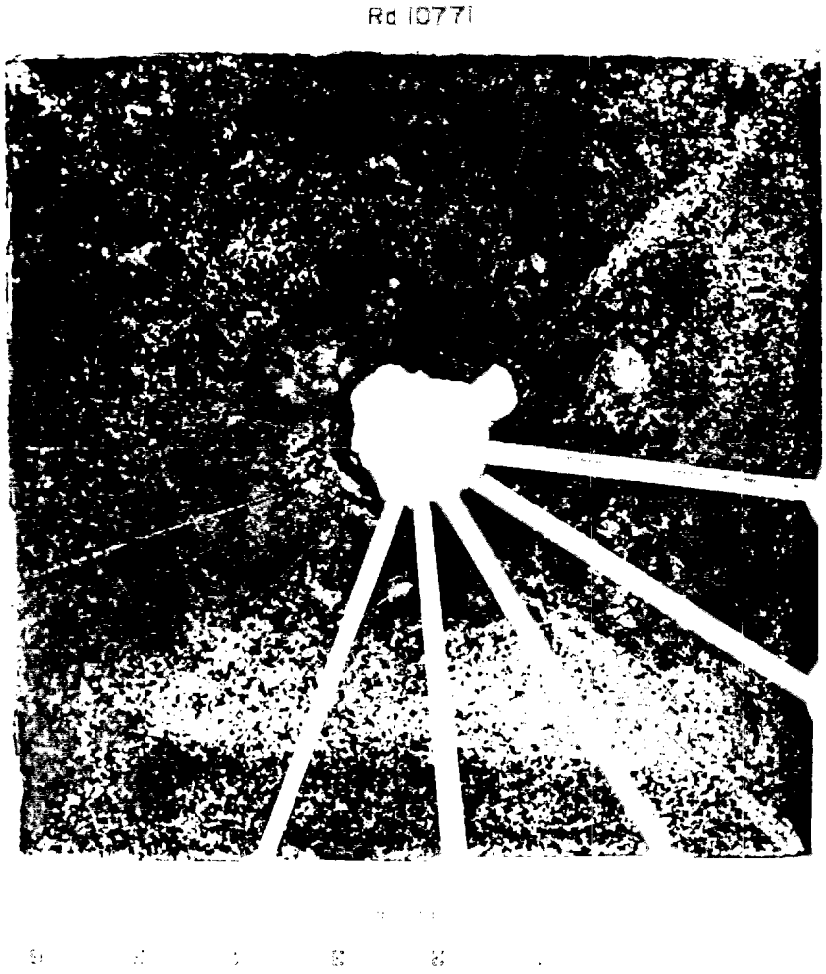

Figure 4. Sectioning of perforated RHA target plate from Rd. 10771.

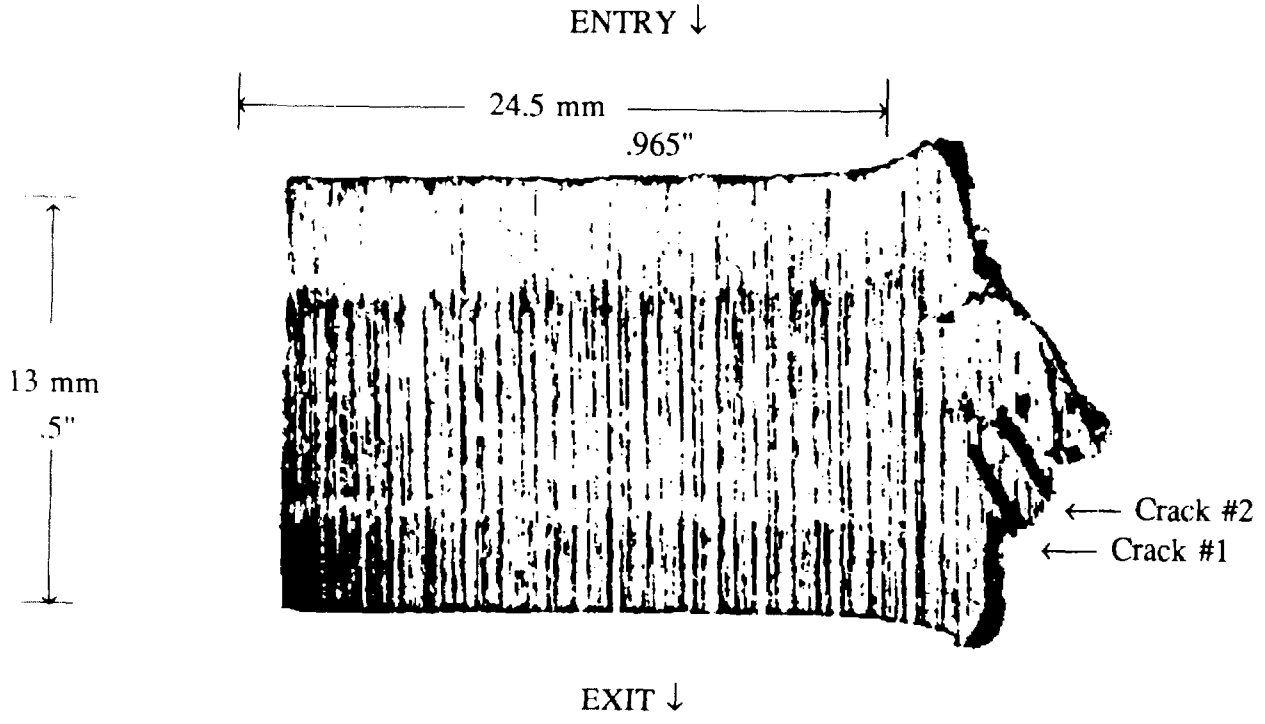

Figure 5. Slice of target plate from Rd. 10771 with two cracks emanating from perforation hole indicated.

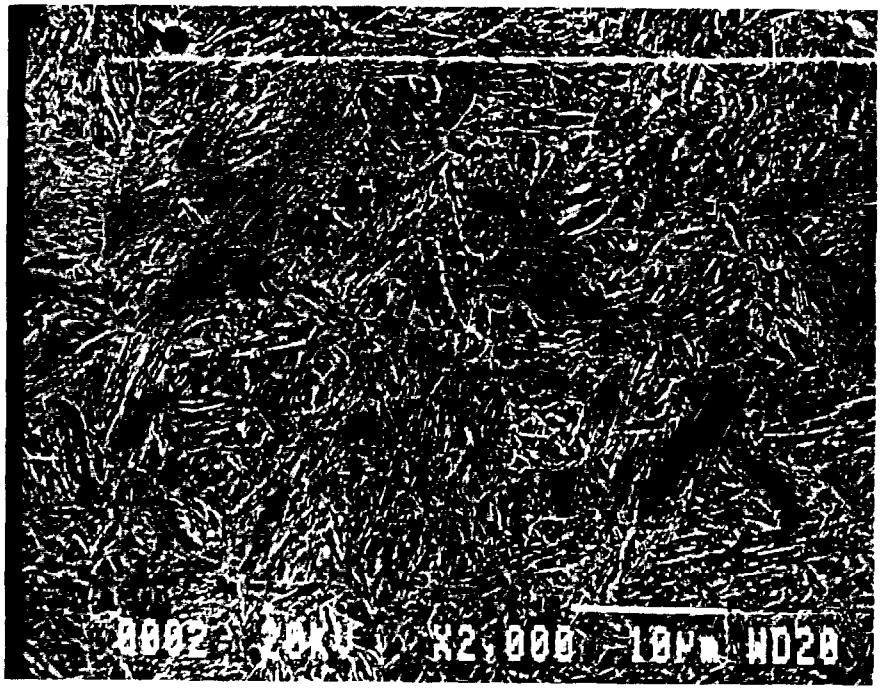

Rd. 10771

Scanning electron micrograph, 2% nital etch, 2000x

Figure 6. Tempered martensite observed in perforated target plate.

Rd. 10771

Optical micrograph,
2% nital etch, 80x

Figure 7. Crack #1 in Figure 5 and adjoining shear band.

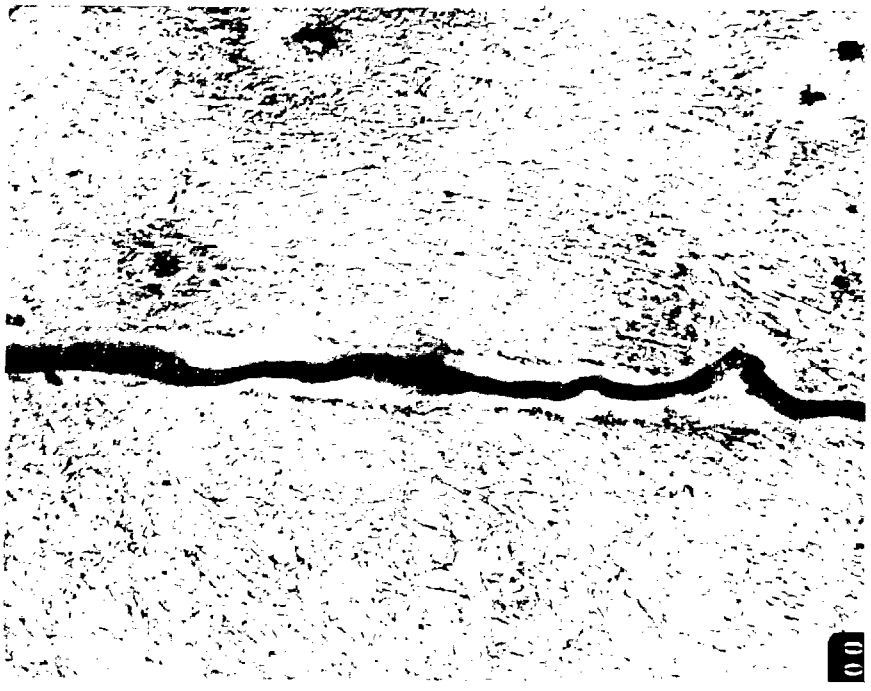

Rd. 10771

Optical micrograph,
2% nital etch, 500x

Figure 8. Enlargement of Figure 7 showing crack to be surrounded by a shear band.

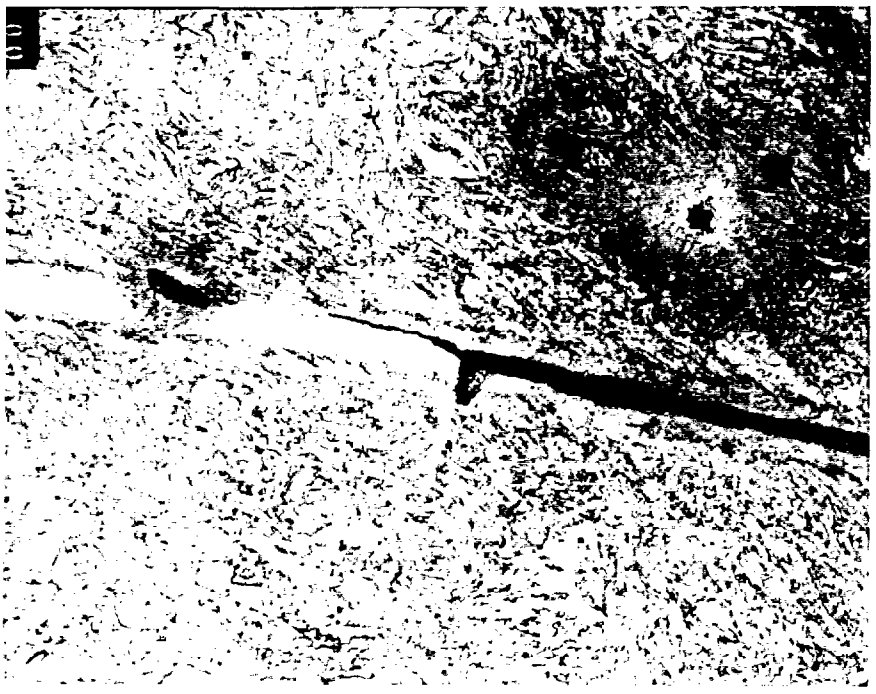

Rd. 10771

Optical micrograph, 2% nital etch, 800x.

Figure 9. Enlargement of Figure 7 showing relationship of crack tip to shear band.

Rd. 10771

Scanning electron micrograph, 2% nital etch, 3,700x.

Figure 10. Further enlargement of Figure 7 showing details of the shear band.

Rd. 10771

Optical micrograph,
2% nital etch, 500x.

Figure 11. Crack #2 in Figure 5 and adjoining shear band.

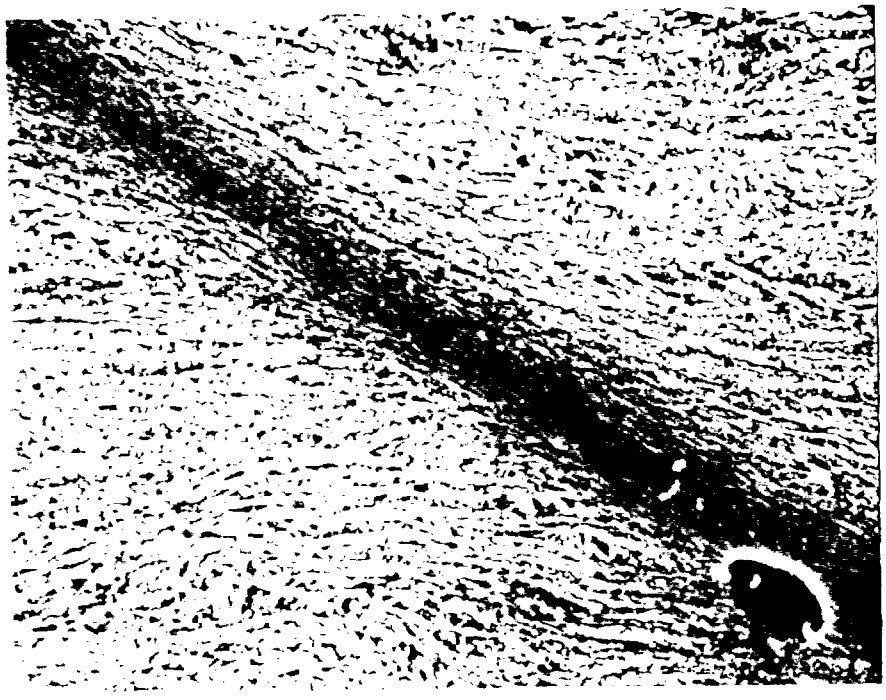

Rd. 10771

Scanning electron micrograph, 2% nital etch, 3,600x.

Figure 12. A shear band with a microstructure similar to that of surrounding martensite.

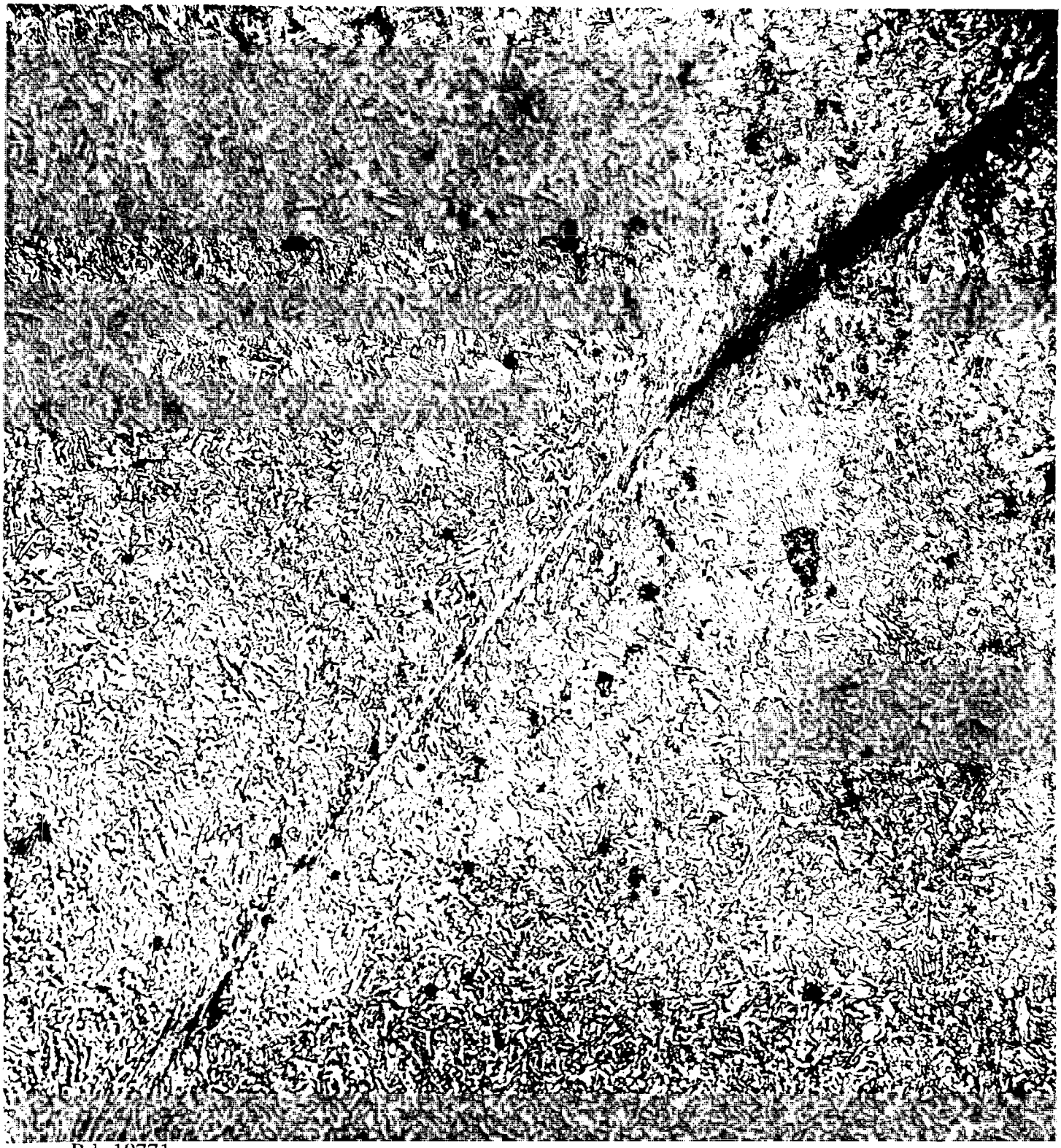

Rd. 10771
Optical micrograph, 2% nital etch, 250x.

Figure 13. A shear band associated with a crack at one end and blending with the ambient martensite at the other.

Rd. 10771

Scanning electron micrograph, 2% nital etch. 4,000x.

Figure 14. Voids have coalesced to form a crack in RHA.

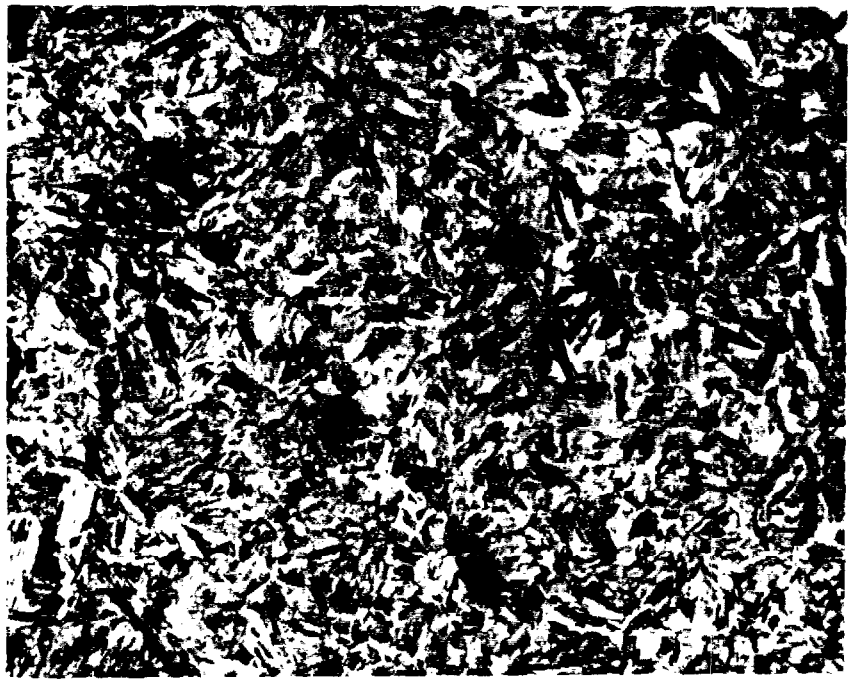

Rd. 4099

Optical micrograph,
2% nital etch, 1,000x.

Figure 15. Lower bainite microstructure in RHA fragment.

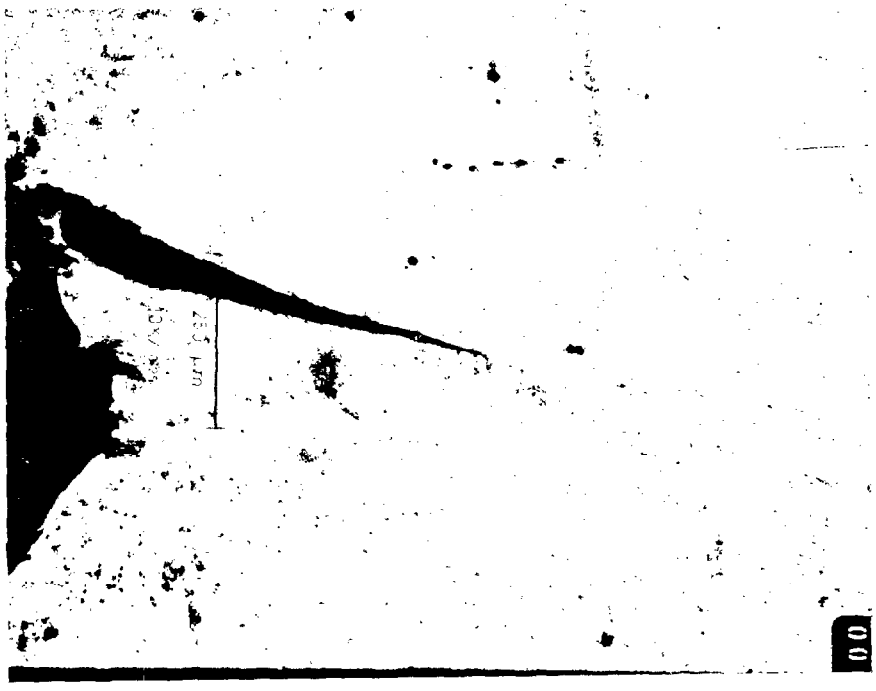

Rd. 4098

Optical micrograph,
2% nital etch, 80x.

Figure 16. Crack at boundary of RHA fragment and adjoining shear band.

Rd. 4100

Optical micrograph,
2% nital etch,
100x.

Figure 17. Shear band that meanders into interior of RHA fragment.

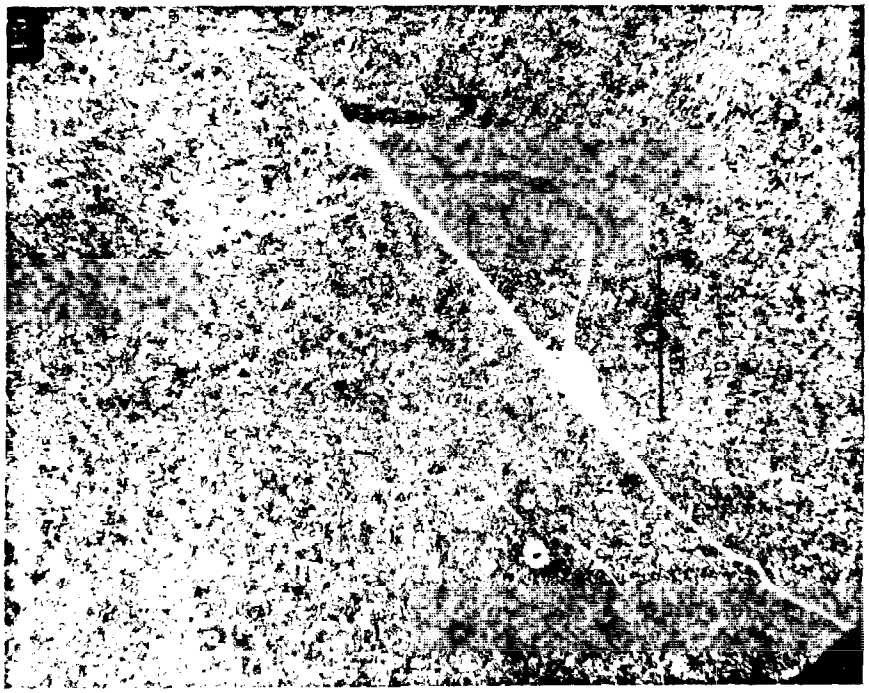

Rd. 4099

Optical micrograph,
2% nital etch, 80x.

Figure 18. Shear band that bifurcates and abruptly changes direction in an RHA fragment.

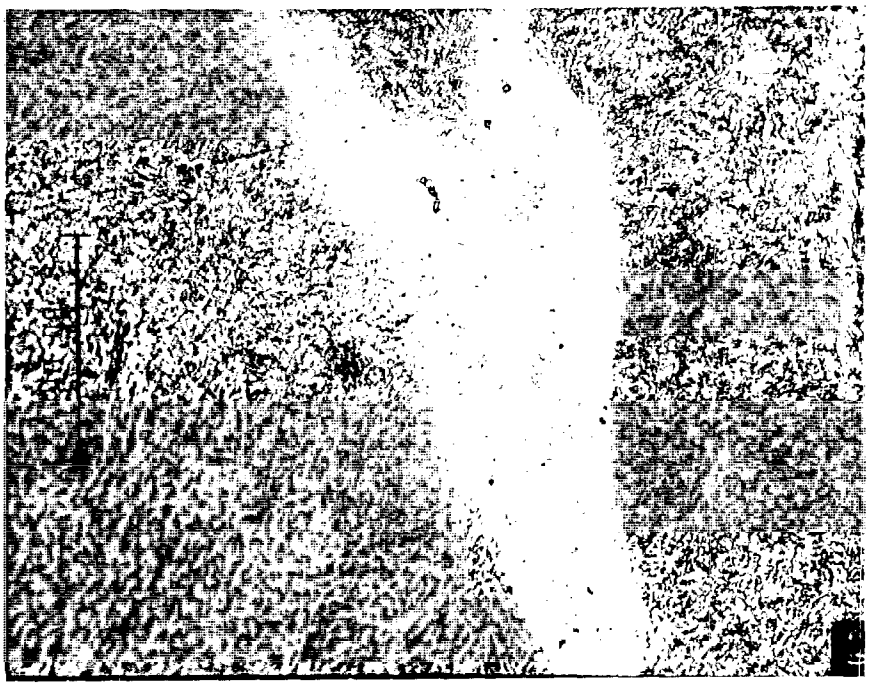

Rd. 4099

Optical micrograph,
2% nital etch, 625x.

Figure 19. Enlargement of Figure 18 in region of shear band bifurcation.

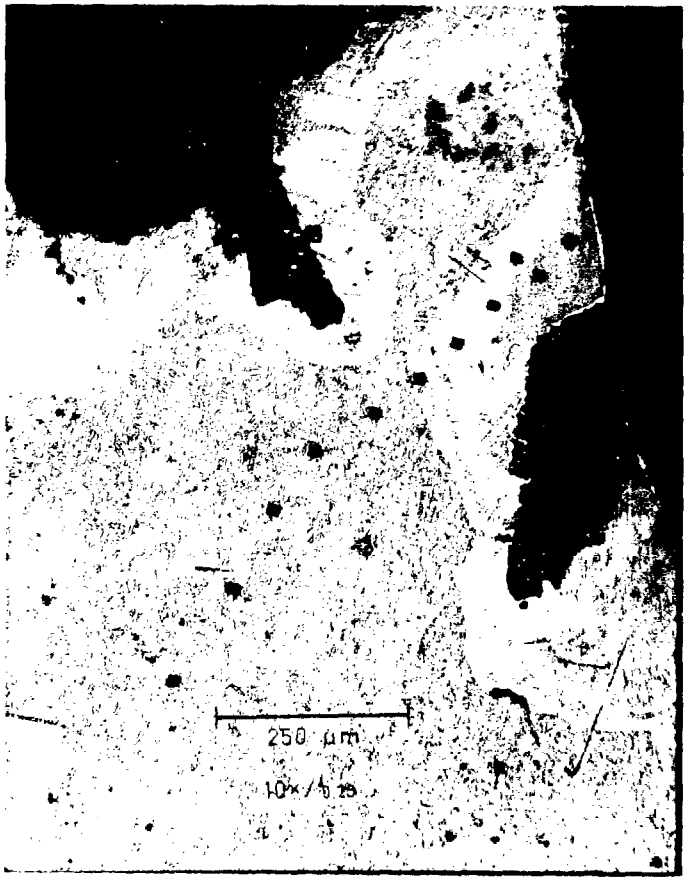

Rd. 4099

Optical micrograph,
2% nital etch, 100x.

Note: Table 2 gives microhardness measurement at indentation points on fragment.

Figure 20. RHA fragment bounded by a band of dendritic structure.

Rd. 4099
Optical micrograph, 2% nital etch, 250x.

Figure 21. Enlargement of Figure 20 with dendritic structure shown.

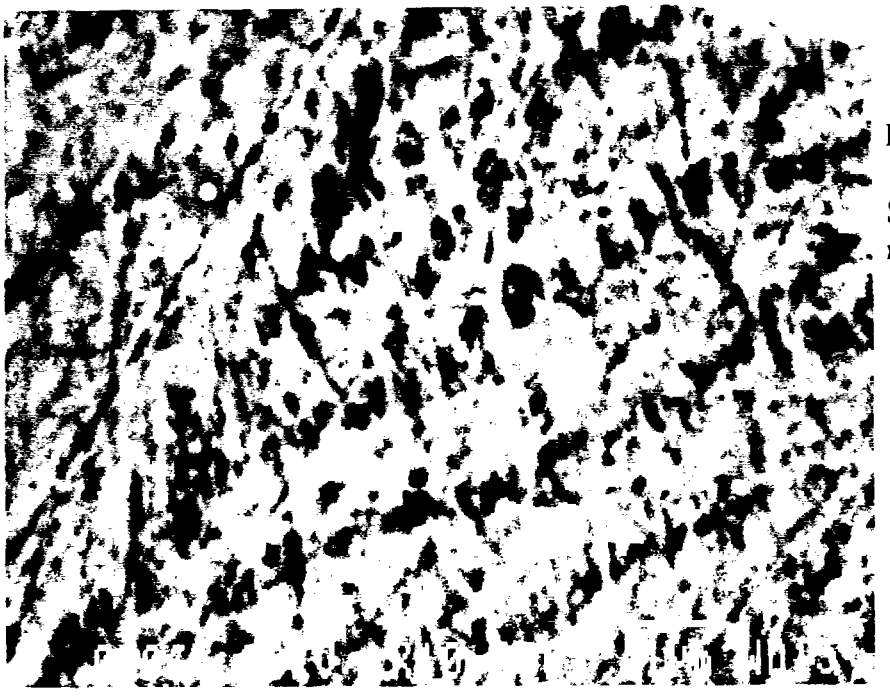

Rd. 4099

Scanning electron micrograph, 2% nital etch, 10,000x.

Figure 22. Further enlargement of dendritic structure in Figure 20.

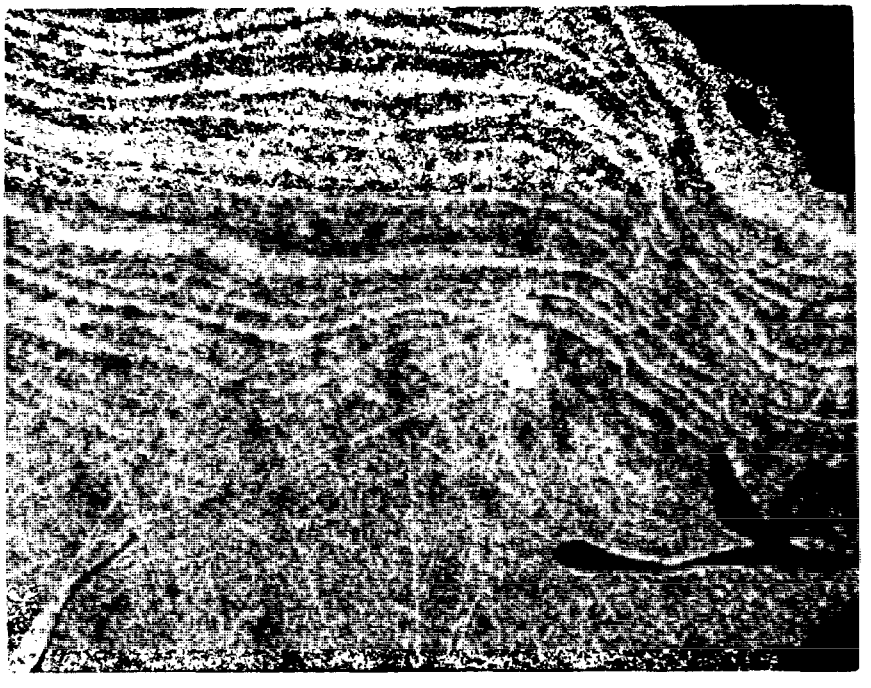

Rd. 4099

Optical micrograph, 2% nital etch, 100x.

Figure 23. Band of striations near RHA fragment's boundary.

Rd. 4099

Optical micrograph,
potassium dichromate etch,
500x.

Figure 24. Copper fragment with variety of grain sizes and evidence of twinning.

INTENTIONALLY LEFT BLANK.

5. REFERENCES

Beatty, J. H., L. W. Meyer, M. A. Meyers, and S. Nemat-Nasser. "Formation of Controlled Adiabatic Shear Bands in AISI 4340 High Strength Steel." MTL-TR-91-4, U. S. Army Materials Technology Laboratory, Watertown, MA, 1990.

Glass, J. T., and W. J. Bruchey, Jr. "Internal Deformation and Energy Absorption During Penetration of Semi-Infinite Targets." Journal of Ballistics, **9**, pp. 2443-2468, 1987.

Hertzberg, R. W. Deformation and Fracture Mechanics of Engineering Materials, Wiley, New York, pp. 121-124, 1976.

Honeycombe, R. W. K. Steels, Microstructure and Properties, Edward Arnold, London, pp. 144-146, 1981.

Meyers, M. A., and K. K. Chawla. Mechanical Metallurgy, Principles and Applications, Prentice-Hall, Englewood Cliffs, NJ, pp. 289-291, 1984.

Moss, G. L. "Shear Strains, Strain Rates and Temperature Changes in Adiabatic Shear Bands." Shock Waves and High-Strain-Rate Phenomena in Metals, edited by M. A. Meyers and L. E. Murr, Plenum Press, New York, pp. 299-312, 1981.

Raftenberg, M. N. "Modeling RHA Plate Perforation by a Shaped Charge Jet." BRL-TR-3363, U. S. Army Ballistic Research Laboratory, Aberdeen Proving Ground, MD, 1992.

Raftenberg, M. N. "Experimental Investigation of Rolled-Homogeneous-Armor Plate Perforation by a Shaped Charge Jet." U. S. Army Research Laboratory, Aberdeen Proving Ground, MD, to be published.

Raftenberg, M. N., and C. D. Krause. "RHA Plate Perforation by a Shaped-Charge Jet; Experiment and Hydrocode Simulation." Shock-Wave and High-Strain-Rate Phenomena in Materials, edited by M. A. Meyers, L. E. Murr and K. P. Staudhammer, Marcel Dekker, New York, pp. 555-564, 1992.

Rogers, H. C., and C. V. Shastry. "Material Factors in Adiabatic Shear Bands in Steels." Shock Waves and High-Strain-Rate Phenomena in Metals, edited by M. A. Meyers and L. E. Murr, Plenum Press, New York, pp. 285-298, 1981.

U. S. Department of Defense. "Military Specification: Armor Plate, Steel, Wrought, Homogeneous (for Use in Combat-Vehicles and for Ammunition Testing)." MIL-A-12560G(MR), U. S. Army Materials Technology Laboratory, Watertown, MA, 1984.

Wittman, C. L., M. A. Meyers, and H.-r. Pak. "Observations of an Adiabatic Shear Band in AISI 4340 Steel by High-Voltage Transmission Electron Microscopy." Metallurgical Transactions A, **21A**, pp. 707-716, 1990.

INTENTIONALLY LEFT BLANK.

No. of Copies	Organization
2	Administrator Defense Technical Info Center ATTN: DTIC-DDA Cameron Station Alexandria, VA 22304-6145
1	Commander U.S. Army Materiel Command ATTN: AMCAM 5001 Eisenhower Ave. Alexandria, VA 22333-0001
1	Director U.S. Army Research Laboratory ATTN: AMSRL-OP-CI-AD, Tech Publishing 2800 Powder Mill Rd. Adelphi, MD 20783-1145
1	Director U.S. Army Research Laboratory ATTN: AMSRL-OP-CI-AD, Records Management 2800 Powder Mill Rd. Adelphi, MD 20783-1145
2	Commander U.S. Army Armament Research, Development, and Engineering Center ATTN: SMCAR-IMI-I Picatinny Arsenal, NJ 07806-5000
2	Commander U.S. Army Armament Research, Development, and Engineering Center ATTN: SMCAR-TDC Picatinny Arsenal, NJ 07806-5000
1	Director Benet Weapons Laboratory U.S. Army Armament Research, Development, and Engineering Center ATTN: SMCAR-CCB-TL Watervliet, NY 12189-4050
(Unclass. only) 1	Commander U.S. Army Rock Island Arsenal ATTN: SMCRI-IMC-RT/Technical Library Rock Island, IL 61299-5000
1	Director U.S. Army Aviation Research and Technology Activity ATTN: SAVRT-R (Library) M/S 219-3 Ames Research Center Moffett Field, CA 94035-1000

No. of Copies	Organization
1	Commander U.S. Army Missile Command ATTN: AMSMI-RD-CS-R (DOC) Redstone Arsenal, AL 35898-5010
1	Commander U.S. Army Tank-Automotive Command ATTN: ASQNC-TAC-DIT (Technical Information Center) Warren, MI 48397-5000
1	Director U.S. Army TRADOC Analysis Command ATTN: ATRC-WSR White Sands Missile Range, NM 88002-5502
1	Commandant U.S. Army Field Artillery School ATTN: ATSF-CSI Ft. Sill, OK 73503-5000
(Class. only) 1	Commandant U.S. Army Infantry School ATTN: ATSH-CD (Security Mgr.) Fort Benning, GA 31905-5660
(Unclass. only) 1	Commandant U.S. Army Infantry School ATTN: ATSH-CD-CSO-OR Fort Benning, GA 31905-5660
1	WL/MNOI Eglin AFB, FL 32542-5000
	Aberdeen Proving Ground
2	Dir, USAMSAA ATTN: AMXSY-D AMXSY-MP, H. Cohen
1	Cdr, USATECOM ATTN: AMSTE-TC
1	Dir, ERDEC ATTN: SCBRD-RT
1	Cdr, CBDA ATTN: AMSCB-CI
1	Dir, USARL ATTN: AMSRL-SL-I
10	Dir, USARL ATTN: AMSRL-OP-CI-B (Tech Lib)

No. of Copies | Organization

5 Director
U.S. Army Research Office
ATTN: J. Chandra
J. Wu
K. Iyer
A. Crowson
Technical Library
P.O. Box 1211
Research Triangle Park, NC 27709-2211

1 Director
U.S. Army Research Laboratory
ATTN: AMSRL-D-TO,
Clarence W. Kitchens, Jr.
Adelphi, MD 20783-1145

1 Commander
U.S. Army Research and Standardization Group (Europe)
ATTN: F. Oertel
P.O. Box 65
FPO NY 09510

8 Director
U.S. Army Research Laboratory - Materials Directorate
ATTN: AMSRL-MA,
G. Bishop
S. Chou
J. Dandekar
A. Rajendran
T. Weerasooriya
M. Wells
J. Beatty
Technical Library
Watertown, MA 02172-0001

1 Commander
U.S. Army Tank-Automotive Command
ATTN: AMSTA-RSK, J. Thompson
Warren, MI 48397-5000

1 U.S. Naval Academy
Department of Mathematics
ATTN: R. Malek-Madani
Annapolis, MD 21402

No. of Copies | Organization

1 Air Force Wright Aeronautical Laboratories
Air Force Systems Command
Materials Laboratory
ATTN: T. Nicholas
Wright-Patterson AFB, OH 45433

4 Commander
U.S. Army Armament Research, Development, and Engineering Center
ATTN: SMCAR-AEE-WW, E. Baker
SMCAR-AET-M,
F. Witt
C. Feng
Technical Library
Picatinny Arsenal, NJ 07806-5000

2 Commander
U.S. Army Missile Command
ATTN: AMSMI-RD, W. Jennings, Jr.
AMSMI-RD-ST-WF, M. Schexnayder
Redstone Arsenal, AL 35898

1 Commander
U.S. Army Tank-Automotive Command
Armor Application Section
ATTN: AMSTA-RSK, S. Goodman
Warren, MI 48397-5000

4 Director
Wright Laboratory
ATTN: WL/MNMW, J.A. Collins
MNW, W. Cook
WL/MNMW, J. Foster, Jr.
Technical Library
Eglin Air Force Base, FL 32542-5434

3 Commander
Naval Surface Warfare Center
ATTN: Technical Library
W. Mock
W. H. Holt
Dahlgren, VA 22448

No. of Copies	Organization
5	Commander Naval Weapons Center ATTN: Code 3266, R. Hoffmann Code 3261, T. Gill S. Finnegan J. C. Schulz Technical Library China Lake, CA 93555-6001
5	Commander Naval Surface Warfare Center ATTN: F. Zerilli H. Chen, U12 H. Mair, R12 C. S. Coffey Technical Library Silver Spring, MD 20903-5000
1	Commander Naval Research Laboratory ATTN: J. A. Nemes Washington, DC 20375
1	Director Defense Advanced Research Projects Agency ATTN: J. Richardson Armor/Antiarmor Joint Program Office Rosslyn, VA 22209-2308
2	Director Defense Advanced Research Projects Agency ATTN: B. Wilcox Tech. Info. 3701 North Fairfax Dr. Arlington, VA 22203-1714
1	Director Defense Advanced Research Projects Agency Land Systems Office ATTN: T. Phillips 3701 North Fairfax Dr. Arlington, VA 22203-1714
1	Office of Munitions ATTN: OUSD(A)/TWD/OM, A. Holt Room 3B1060, The Pentagon Washington, DC 20301

No. of Copies	Organization
1	Commander Naval Postgraduate School ATTN: Code 73, J. Sternberg Monterey, CA 93943
12	Director Sandia National Laboratories ATTN: D. Grady M. Kipp W. Herrmann S. Passman M. Forrestal V. Luk L. Davison P. Yarrington S. A. Silling J. M. McGlaun E. Hertel M. M. Hightower P.O. Box 5800 Albuquerque, NM 87185-5800
1	Director Sandia National Laboratories ATTN: D. Bammann Livermore, CA 94550
1	National Institute of Science and Technology ATTN: T. Burns Technology Building, Rm A151 Gaithersburg, MD 20899
11	Director Lawrence Livermore National Laboratory ATTN: L-38, M. Finger L-122, B. Bowman L-35, R. Couch R. Tipton D. Baum D. Steinberg J. Reaugh L342, D. Lassila, G. Goudreau W. H. Gourdin Technical Library P.O. Box 808 Livermore, CA 94550

No. of Copies | Organization

16 Director
Los Alamos National Laboratory
ATTN: J. Chapyak
MS F663,
J. Johnson
S. K. Shiferl
T. F. Adams
D. A. Mandell
P. Follansbee
MS J960,
R. Karpp
L. Hull
MS B216, J. W. Hopson
MS B295,
K. Holian
G. T. Gray
MS K765, S. R. Chen
MS G787, G. E. Cort,
J. Repa
A. K. Zurek
Technical Library
P. O. Box 1663
Los Alamos, NM 87454

1 Brown University
Division of Engineering
ATTN: R. Clifton
Providence, RI 02912

1 University of California at Santa Barbara
Department of Materials Science
ATTN: A. Evans
Santa Barbara, CA 93106

4 University of California at San Diego
Department of Applied Mechanics and Engineering Sciences
ATTN: R. Asaro
K. Vecchio
M. Meyers
S. Nemat-Nasser
La Jolla, Ca 92093

2 California Institute of Technology
ATTN: W. Knauss
G. Ravichandran
Mail Code 105-50
Pasadena, CA 91125

No. of Copies | Organization

1 Michigan Technological University
Dept. of Mechanical Engineering
ATTN: W. W. Predebon
1400 Townsend Dr.
Houghton, MI 49931-1295

1 Cornell University
Department of Theoretical and Applied Mechanics
ATTN: J. Jenkins
Ithaca, NY 14850

2 Drexel University
Department of Materials Engineering
ATTN: H. Rogers
P. Chou
Philadelphia, PA 18104

1 Harvard University
Division of Engineering and Applied Physics
ATTN: J. Hutchinson
Cambridge, MA 02138

1 University of Illinois
Department of Theoretical and Applied Mechanics
ATTN: T. Shawki
Urbana, IL 61801

3 The Johns Hopkins University
Department of Mechanical Engineering
Latrobe Hall
ATTN: A. Douglas
K. Ramesh
W. Sharp
34th and Charles Streets
Baltimore, MD 21218

2 University of Maryland
Department of Mechanical Engineering
ATTN: R. Armstrong
J. Dally
College Park, MD 20742

1 University of Maryland Baltimore County
ATTN: A. Khan
Baltimore, MD 21228

No. of Copies	Organization
1	Massachusetts Institute of Technology Department of Mechanical Engineering ATTN: L. Anand Cambridge, MA 02139
1	University of Missouri-Rolla Department of ME, AE & EM ATTN: R. Batra Rolla, MO 65401-0249
1	State University of New York at Stony Brook Department of Applied Mathematics and Statistics ATTN: J. Glimm Stony Brook, NY 11794
1	North Carolina State University Department of Mechanical and Aerospace Engineering ATTN: M. Zikry Raleigh, NC 27695
1	Northwestern University Department of Applied Mathematics ATTN: W. Olmstead Evanston, IL 60208
1	Northwestern University Department of Civil Engineering ATTN: T. Belytschko Evanston, IL 60208
1	Rensselaer Polytechnic Institute Department of Mechanical Engineering ATTN: E. Krempl Troy, NY 12181
1	Rensselaer Polytechnic Institute Department of Computer Science ATTN: J. Flaherty Troy, NY 12181
1	University of Texas Texas Institute for Comp. Mechanics ATTN: J. Oden Austin, TX 78712

No. of Copies	Organization
1	Texas A&M University Aerospace Engineering Department ATTN: T. Strouboulis College Station, TX 77843-3141
1	Washington State University Department of Mechanical and Materials Engineering ATTN: H. Zbib Pullman, WA 99164
1	Institute for Defense Analysis ATTN: G. Mayer 1801 N. Beauregard Street Alexandria, VA 22311
4	SRI International ATTN: D. Curran R. Shockey L. Seaman H. Giovanola 333 Ravenswood Avenue Menlo Park, CA 94025
3	Southwest Research Institute Department of Mechanical Sciences ATTN: C. Anderson J. Lankford U. Lindholm 8500 Culebra Road San Antonio, TX 02912
1	Baltimore Gas and Electric Company ATTN: Ms. Claire D. Krause Fort Smallwood Road Complex 1000 Brandon Shores Road Baltimore, MD 21226
1	California Research and Technology, Inc. ATTN: D. Orphal 5117 Johnson Dr. Pleasanton, CA 94566
2	General Research Corporation ATTN: A. Charters T. Menna 5383 Hollister Ave. Santa Barbara, CA 93111

No. of Copies	Organization
3	Alliant Techsystems, Inc. ATTN: G. Johnson T. Holmquist C. L. Wittman 7225 Northland Dr. Brooklyn Park, MN 55428
1	Research & Development Associates ATTN: J. Furlong 2100 Washington Blvd. Arlington, VA 22209
1	Aluminum Company of America ATTN: R. Stemler ALCOA Center, PA 15069
2	E.I. DuPont de Nemours ATTN: M. Bernhardt, B. Scott P.O. Box 80702 Wilmington, DE 19880
1	General Dynamics Land Systems Division ATTN: W. Burke P.O. Box 1800 Warren, MI 48090
2	Kaman Sciences Corporation ATTN: J. May M. Normandia P.O. Box 7643 Colorado Springs, CO 80933
2	California Research and Technology, Inc. ARAP Group - A Titan Company ATTN: R. Thorpe M. Majerus P.O. Box 2229 Princeton, NJ 08543-2229
1	Battelle Ordnance Systems and Technology Department ATTN: D. Butz 505 King Ave. Columbus, OH 43201-2693

No. of Copies	Organization
2	Battelle Edgewood Operations ATTN: R. Jameson S. Gołaski 2113 Emmorton Park Rd. Edgewood, MD 21040
1	GTE Products Corporation Chemical and Metallurgical Division ATTN: J. Gonzalez Hawes St. Towanda, PA 18848
1	Teledyne-Brown Engineering ATTN: L. Smalley, MS50 P.O. Box 07007 Huntsville, AL 35807-7007
1	Failure Analysis Associates ATTN: S. Andrew P.O. Box 3015 Menlo Park, CA 94025
2	Lanxide Armor Products, Inc. ATTN: V. Kelsey K. Leighton P.O. Box 6077 Newark, DE 19714-6077
1	Dyna East Corporation ATTN: W. Flis 3201 Archer St. Philadelphia, PA 19104
1	Institute for Advanced Technology ATTN: S. Bless 4030-2 W. Braker Lane Austin, TX 78759-5329
1	Zernow Technical Services, Inc. ATTN: L. Zernow 425 West Benita, Suite 208 San Dimas, CA 91773
1	Orlando Technology, Inc. ATTN: D. Matuska P.O. Box 855 Shalimar, FL 32579

No. of Copies	Organization
1	Denver Research Institute ATTN: J. D. Yatteau P.O. Box 10127 Denver, CO 80210
1	Livermore Software Technology Corporation ATTN: J. Hallquist 2876 Waverly Way Livermore, CA 94550
1	University of Illinois Dept. of Metallurgy and Mineral Engineering ATTN: H.-r. Pak Urbana, IL 61801

No. of Copies	Organization
1	Ruhr-Universitat Bochum ATTN: J. Kalthoff Universitatstrasse 150 4360 Bochum 1, Postfach 102148 GERMANY
1	Condat GmbH ATTN: K. Thoma Maximilianstrasse 28 8069 Scheyern-Fernhag GERMANY
1	IFAM Materialforschung ATTN: L. Meyer Lesumer Heerstrasse 36 2820 Bremen 77 GERMANY
2	RARDE ATTN: I. Cullis A. Hopkins Fort Halstead - Sevenoaks TN14 7BP Kent ENGLAND
1	Defence Research Establishment Suffield ATTN: C. Weickert Ralston, Alberta, TOJ 2NO Ralston CANADA
1	Defence Research Establishment Valcartier ATTN: N. Gass P.O. Box 8800 Courcellette, PQ, GOA 1RO CANADA
1	Canadian Arsenals, LTD ATTN: P. Pelletier 5 Montee des Arsenaux Villie de Gardeur, PQ, J5Z2 CANADA
1	Centre d'Extudes de Gramat ATTN: Solve, G. 46JO Gramat FRANCE

No. of Copies	Organization
1	Ernst-Mach Institut ATTN: A. Stilp Eckerstrasse 4 D-7800 Freiburg i. Br. GERMANY
1	IABG ATTN: H. Raatschen Einsteinstrasse 20 D-8012 Ottobrun B. Muenchen GERMANY
1	Centre d'Etudes de Vajours ATTN: PLOTARD J.-P. Boite Postale No. 7 77181 Country FRANCE
1	PRB S.A. ATTN: M. Vansnick Avenue de Tervueren 168, Bte. 7 Brussels, B-1150 BELGIUM
1	AB Bofors/Ammunition Division ATTN: Jan Hasslid Box 900 S-691 80 Bofors SWEDEN
1	Materials Research Laboratories ATTN: R. L. Woodword P.O. Box 50 Ascot Vale Victoria 3032 AUSTRALIA
1	E. Hisch MIL P.O. Box 02128 ISRAEL
1	Y. Kivity Rafael Ballistics Center Haifa ISRAEL

USER EVALUATION SHEET/CHANGE OF ADDRESS

This Laboratory undertakes a continuing effort to improve the quality of the reports it publishes. Your comments/answers to the items/questions below will aid us in our efforts.

1. ARL Report Number ARL-MR-68 Date of Report June 1993

2. Date Report Received _____

3. Does this report satisfy a need? (Comment on purpose, related project, or other area of interest for which the report will be used.) _____

4. Specifically, how is the report being used? (Information source, design data, procedure, source of ideas, etc.) _____

5. Has the information in this report led to any quantitative savings as far as man-hours or dollars saved, operating costs avoided, or efficiencies achieved, etc? If so, please elaborate. _____

6. General Comments. What do you think should be changed to improve future reports? (Indicate changes to organization, technical content, format, etc.) _____

CURRENT ADDRESS

_____
Organization

_____
Name

_____
Street or P.O. Box No.

_____
City, State, Zip Code

7. If indicating a Change of Address or Address Correction, please provide the Current or Correct address above and the Old or Incorrect address below.

OLD ADDRESS

_____
Organization

_____
Name

_____
Street or P.O. Box No.

_____
City, State, Zip Code

(Remove this sheet, fold as indicated, tape closed, and mail.)

(DO NOT STAPLE)

DEPARTMENT OF THE ARMY

OFFICIAL BUSINESS

BUSINESS REPLY MAIL
FIRST CLASS PERMIT No 0001, APG, MD

Postage will be paid by addressee.

Director
U.S. Army Research Laboratory
ATTN: AMSRL-OP-CI-B (Tech Lib)
Aberdeen Proving Ground, MD 21005-5066

NO POSTAGE
NECESSARY
IF MAILED
IN THE
UNITED STATES